

Development of a critical-angle transmission grating spectrometer for the International X-Ray Observatory

Ralf K. Heilmann, Minseung Ahn, Mark W. Bautz, Rick Foster, David P. Huenemoerder, Herman L. Marshall, Pran Mukherjee, Mark L. Schattenburg, Norbert S. Schulz, and Matthew Smith

MIT Kavli Institute for Astrophysics and Space Research,
Massachusetts Institute of Technology,
77 Massachusetts Avenue, Cambridge, Massachusetts 02139, USA

ABSTRACT

We present a high-resolution soft x-ray grating spectrometer concept for the International X-Ray Observatory (IXO) that meets or exceeds the minimum requirements for effective area ($> 1,000 \text{ cm}^2$ for $E < 1 \text{ keV}$) and spectral resolution ($E/\Delta E > 3,000$). At the heart of the spectrometer is an array of recently developed high-efficiency blazed transmission gratings, the so-called critical-angle transmission (CAT) gratings. They combine the advantages of traditional transmission gratings (very low mass, extremely relaxed alignment and flatness tolerances) with those of x-ray reflection gratings (high efficiency due to blazing in the direction of grazing-incidence reflection). In addition, a CAT grating spectrometer is well-suited for co-existence with energy-dispersive high-energy focal plane detectors, since most high-energy x rays are neither absorbed, nor diffracted, and contribute to the effective area at the telescope focus. Since our initial successful x-ray demonstrations of the CAT grating concept with large-period and lower aspect-ratio prototypes, we have now microfabricated 200 nm-period silicon CAT gratings comprised of grating bars with the required dimensions (6 micron tall, 40 nm wide, aspect ratio 150), optimized for the 0.3 to 1.0 keV energy band. Preliminary analysis of recent x-ray tests show blazing behavior up to 1.28 keV in accordance with predictions.

Keywords: x-ray optics, International X-ray Observatory, IXO, critical-angle transmission grating, x-ray spectroscopy, blazed transmission grating, extreme ultraviolet, soft x-ray

1. INTRODUCTION

The grating spectrometers on Chandra and XMM-Newton have revolutionized x-ray spectroscopy for high-energy astrophysics.¹ Both observatories are still operational after ten years in space, but a successor mission is overdue. Recently NASA, ESA, and JAXA have joined previously independent efforts (Constellation-X and XEUS) to develop such a mission, named the International X-ray Observatory (IXO).² IXO is designed to enable high-collecting-area spectroscopy over a wide band (from 0.3 to 40 keV), which can not be provided by a single instrument. A grating spectrometer is baselined to meet the current science requirements of resolution $R = E/\Delta E > 3000$ and effective area $> 1,000 \text{ cm}^2$ over the soft x-ray band of 0.3 to 1.0 keV. The science addressed by this instrument ranges from the large scale structure of the universe to the detailed structure of individual stars. Soft x-ray spectroscopy is needed to resolve the absorption and emission signatures of atomic ions which reveal the temperatures, compositions, and dynamics of the plasmas involved. Examples are detection of the warm/hot intergalactic medium (WHIM) - the “missing baryons”³ - through absorption line studies toward distant galaxies,⁴ detection of flows in the galactic and intergalactic media, absorption edge structure studies from gas and dust in the Interstellar Medium,⁵ and the study of emission anomalies in the spectra of young stars.⁶

In the following we present a transmission grating spectrometer concept centered on high-efficiency, blazed transmission gratings,⁷ the so-called critical-angle transmission (CAT) gratings.^{8,9} The spectrometer concept is based on the Chandra High Energy Transmission Grating Spectrometer (HETGS)¹⁰ and adapted for blazed

Further author information: Send correspondence to R.K.H. E-mail: ralf@space.mit.edu, URL: <http://snl.mit.edu/>

transmission. We will first briefly review the CAT grating concept, followed by a description of the optical design philosophy, a summary of recent configuration studies, and finally by a discussion of new grating fabrication and x-ray test results on 200 nm-period CAT gratings.

2. THE CRITICAL-ANGLE TRANSMISSION (CAT) GRATING

Traditional phase-shifting transmission gratings such as those flown on the Chandra HETGS rely on the interference of wavefronts that have undergone π differential phase shifts upon transmission through a membrane-supported grating.¹⁰ Peak efficiency can be designed for a specific wavelength. However, soft x rays are readily absorbed in even tens-of-nanometers-thin layers of matter, which strongly reduces the diffraction efficiency of a phase-shifting transmission grating across many wavelengths. In CAT gratings transmission occurs predominantly though vacuum, and path length differences that lead to diffraction are generated via highly efficient grazing-incidence reflection (below the critical angle of total external reflection) off of the ultra-smooth sidewalls of high aspect ratio grating bars.^{8,9} CAT gratings can therefore achieve diffraction efficiencies on the order of 50 % over a broad band that rival those of grazing incidence reflection gratings in the off-plane mount.¹¹⁻¹⁵

For soft x rays, where grating diffraction angles for useful diffraction orders are usually on the order of only a few degrees, transmission gratings have the added advantage that they can be orders of magnitude more alignment and figure insensitive in certain degrees of freedom than reflection gratings. Transmission gratings also only need to be a few micrometers thick and therefore have very little mass compared to long grazing-incidence reflection gratings.

Fig. 1 shows a schematic cross section through a freestanding CAT grating. The grating bars are only supported on their sides by a coarse support mesh (not shown). Photons are incident onto the grating bar sidewalls at some angle α below the critical angle for total external reflection, θ_c . Every x ray incident upon the space between grating bars undergoes a single reflection. Thus the optimum grating depth d should be $d = a/\tan \alpha$, with a being the space between two neighboring grating bars. Grating bar thickness b should be as small as reasonably possible to minimize absorption or blockage of x rays. The grating bar sidewalls need to be of nm roughness or less to minimize scattering losses. For soft x rays θ_c is typically on the order of $1 - 5^\circ$.

The grating equation gives the angles β_m at which the m^{th} diffracted order is observed when a wave of wavelength λ is incident onto a periodic structure with period p at an angle α . The angles are defined relative to the normal of the direction of periodicity in the plane of incidence:

$$\frac{m\lambda}{p} = \sin \alpha - \sin \beta_m, \quad (1)$$

with $m = 0, \pm 1, \pm 2, \dots$. In order for β_m to be reasonably large for small m and for soft x rays the grating period needs to be on the order of a few hundred nm or less. A set of parameters that describes one possible design for a CAT grating-based transmission grating spectrometer that fulfills IXO requirements is $p = 200$ nm, $b = 40$ nm, $\alpha = 1.5^\circ$, which leads to $d = 6110$ nm, and a high aspect ratio of $d/b \approx 150$ for the grating bars. If the grating bar sidewall microroughness is below ~ 1 nm the walls act as efficient silicon mirrors.

The grating equation gives no information on the diffraction efficiency in each order. We have previously introduced a simple model - based on the Fraunhofer approximation of scalar Kirchhoff diffraction theory¹⁶ - that provides a simplified, but intuitive understanding of the intensity distribution in an idealized CAT grating.^{8,9,17} Basically a CAT grating can be approximated as an amplitude grating with a blaze envelope of width proportional to λ/a . The blaze envelope modulates the intensity of the diffraction peaks, is centered in the direction of specular reflection from the grating bar sidewalls, and is reduced by the specular reflectivity of the sidewalls. Upon rotation of the grating relative to incident x rays the blaze envelope will move in accordance with the laws of mirror reflection, but the angles of the transmitted diffraction orders will change much less, being governed by the grating equation.⁸

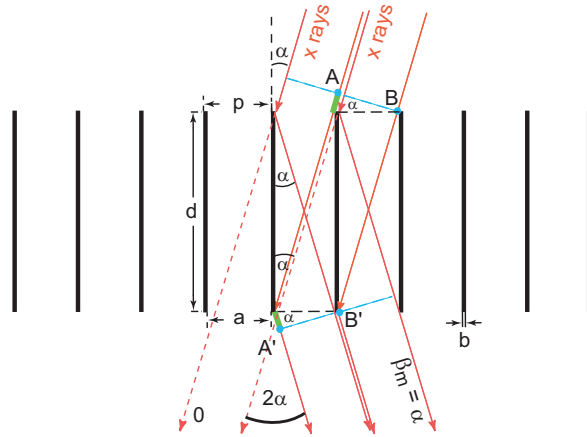


Figure 1. Schematic cross section through a CAT grating. The m^{th} diffraction order occurs at an angle β_m where the path length difference between AA' and BB' is $m\lambda$. Shown is the case where β_m coincides with the direction of specular reflection from the grating bar sidewalls ($\beta_m = \alpha$), i.e., blazing in the m^{th} order.

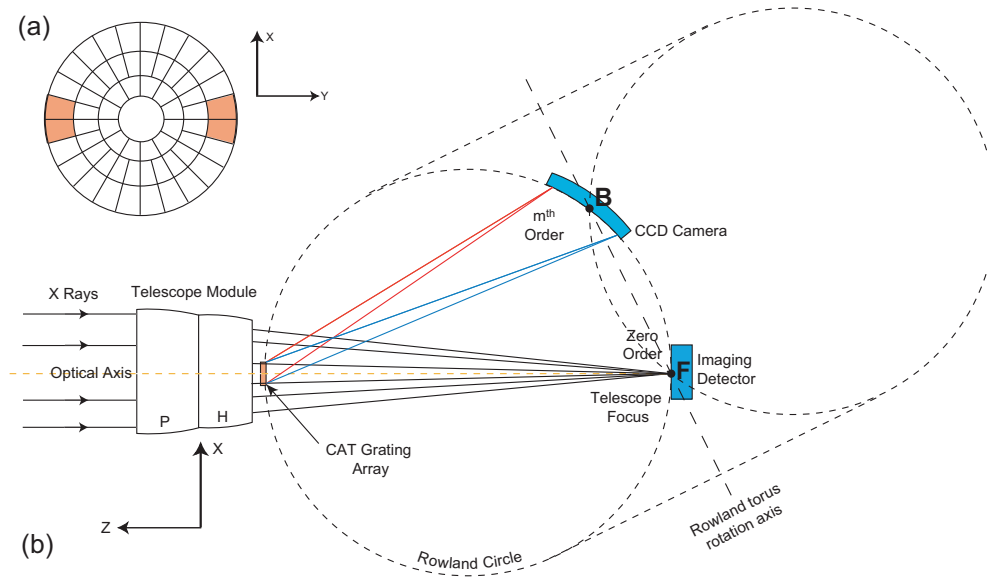


Figure 2. Schematic of CAT grating spectrometer. (a) View of the Flight Mirror Assembly (FMA) in the +Z direction. Four outer ring modules (shaded) are covered by gratings. (b) Schematic of optical design (not to scale). X rays are focused by the parabolic (P) and hyperbolic (H) mirror shells of the segmented Wolter-I optic on the point F. CAT gratings intercept a fraction of the x rays and diffract them predominantly at angles centered around the blaze direction. Representative paths for longer (red) and shorter (blue) wavelength rays diffracted in m^{th} order are shown. See text for more detail.

3. CAT GRATING SPECTROMETER (CATGS) DESIGN

The optical design of the CATGS is based on the design for the Chandra HETGS.¹⁰ Flat transmission grating facets are placed in the converging beam of the telescope on the surface of a Rowland torus that contains the telescope focus. First considering only on-axis x rays in the x-z plane of Fig. 2 arriving from infinity and converging at the focus F, all facets in the x-z plane are oriented such that their normals have the same angle relative to x rays hitting the center of every facet.

This simple construct guarantees that every x ray of wavelength λ that hits the center of a facet and is

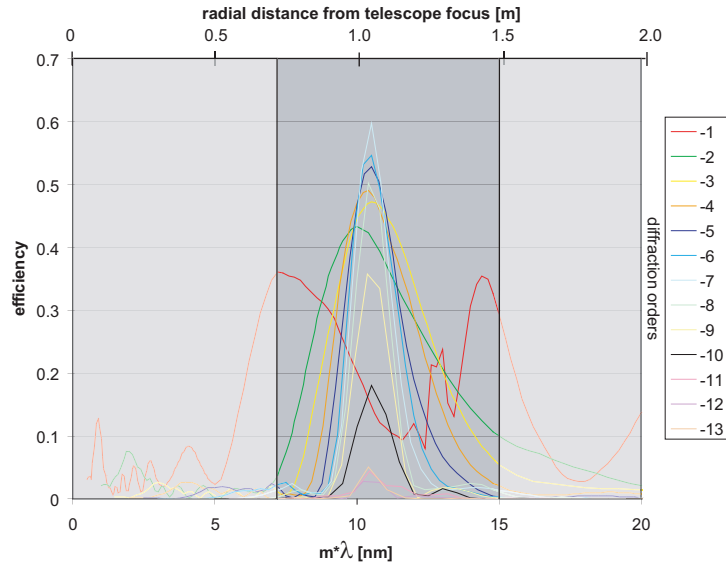


Figure 3. Plot of 200 nm-period CAT grating diffraction efficiency (from RCWA predictions) for orders -1 through -13 as a function of $m\lambda$ (bottom axis) or radial distance from telescope focus (\sim along the dispersion direction on the CCD array; top axis). Except for the -1st order, which is affected by the silicon L-edge, the diffraction efficiency for all orders peaks around 10.5 nm in $m\lambda$ space (or 3° from the incident direction in real space) due to blazing. The camera CCDs must be able to distinguish between x-ray energies from different diffracted orders that land on the same CCD pixel. The dark shaded region ($7.8 \text{ nm} \leq m\lambda \leq 15 \text{ nm}$) is captured by the CCD array.

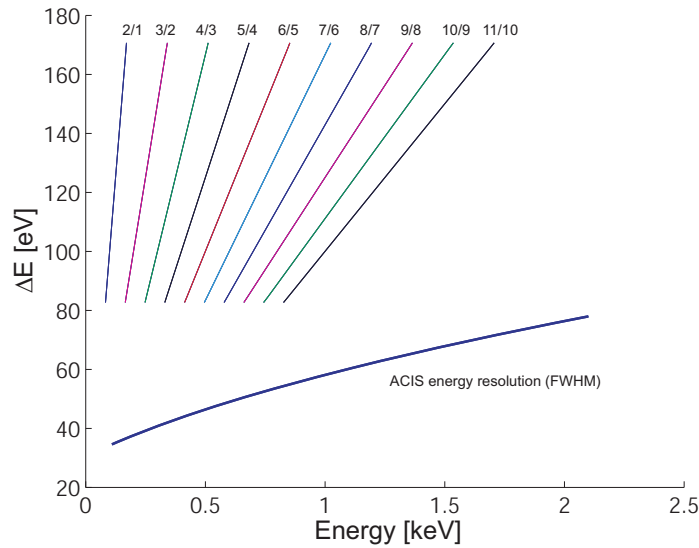


Figure 4. Energy difference between different diffraction orders ($m + 1/m$) as a function of energy for gratings with $p = 200$ nm. Values are only shown for those x rays that land on the CCD array. The blaze condition corresponds to $\Delta E = 118$ eV. For comparison the energy resolution of an ACIS type CCD on Chandra is shown.¹⁸

diffracted in m^{th} order will converge to a single point on the Rowland circle. We will therefore obtain a focused diffraction spectrum along the Rowland circle. A Rowland torus can be constructed by selecting the point B in the spectrum that corresponds to the direction of the peak of the CAT grating blaze envelope and rotating the Rowland circle around an axis that contains points B and F. Now all converging on-axis rays that hit the center of any grating facet on the Rowland torus and get diffracted in the blaze peak direction will converge at point B. Rays that hit other parts of a grating facet will be slightly defocused, but defocus in the cross-dispersion direction is unimportant, and defocus in the dispersion direction can be compensated through slight variation of the grating period across a facet (“chirping”). Rays with wavelengths that diffract away from the blaze peak will also be slightly defocused, but mostly in the cross-dispersion direction. For the spectral resolution $R = E/\Delta E$ or $\lambda/\Delta\lambda$, which is dominated by the 5 arcsec point-spread function (PSF) of the IXO telescope, these aberrations will play a minor role. A simple estimate of the PSF-limited resolution at blaze for gratings close to the focal length from focus is given by twice the reflection angle off the grating sidewalls ($2 \times 1.5^\circ = 3.0^\circ$) from the incident beam, divided by the PSF: $R \sim 3^\circ/5 \text{ arcsec} = 2160$. At some wavelengths two or more orders will contribute significantly to the diffraction efficiency, with the higher order having higher spectral resolution and the lower order having lower resolution. Weighting the resolution for each wavelength by the relative efficiencies of its blazed orders leads to an average spectral resolution close to the same value as above over a broad band.⁷

The spectral resolution can be increased through sub-aperturing of the grazing-incidence Wolter I optic,¹⁹ i.e., by limiting the grating coverage of the mirrors in the azimuthal direction to two opposing 30° segments. This leads to an hour-glass shaped PSF in the diffraction spectrum. The dispersion direction is aligned along the narrowest part of the PSF, thereby decreasing the $\Delta\lambda$ for which spectral lines can be separated. Ray traces interpolated from Constellation-X studies⁷ predict spectral resolution well above 3000 (half energy width) over the 1-5 nm band in this case. The Rowland torus geometry described above is by no means the only possible implementation of a CATGS that meets the resolution requirements, and further IXO-specific CATGS ray trace studies are in progress.

The detector that records the diffracted rays only extends over the main part of the blaze envelope (see Fig. 3). Our baseline consists of a linear array of 32 CCDs that does not interfere with other focal plane instruments and can therefore be operated simultaneously with them. There is a tradeoff between the length of the array and the order-sorting capability of the CCDs: Larger grating period p – and thus larger gap a – leads to a narrower blaze envelope, resulting in a shorter CCD array, but for a given blaze angle this puts more and higher diffraction orders on the detector. Since the energy difference ΔE between spatially overlapping orders is smaller for a grating with larger period, the CCDs must be able to distinguish between x rays with smaller ΔE . Even though we have demonstrated patterning of gratings with periods of 100 nm and 50 nm,^{20,21} a period of 200 nm appears to be a good compromise between detector size and order-sorting capability (see Fig. 4).

4. CATGS CONFIGURATION STUDIES

Since the switch from Constellation-X to IXO a number of detailed configuration studies for a CATGS design were performed, resulting in a strawman design briefly described in the following.

The CATGS consists of two main parts: An assembly of grating facets near the aft end of the telescope mirrors, and a CCD camera with support electronics at the fixed instrument platform (FIP) near the focal plane (see Fig. 5).

The Camera Assembly (CA) is mounted via an interface adapter to a focus mechanism (focus tolerance: better than 0.5 mm), which in turn is connected to the FIP. The Camera Assembly holds the CCD array, which connects to the Detector Electronics Assembly (DEA) via harnesses between connector panels on the CA and DEA. The DEA connects to a Digital Processing Assembly (DPA), which performs data processing on DEA generated image frames, via x-ray event extraction algorithms. The CA holds a cooled focal plane (-90° C) made up of 32 CCID41-based²² back illuminated framestore style CCDs ($25 \times 25 \text{ mm}^2$, 25 micron pixels). The CCDs are mounted in a 1x32 configuration that approximates the Rowland circle defined by the GAS and the telescope focus (see also Fig. 6).

Fig. 7 gives an overview of the structural hierarchy for the grating assembly. The grating facets are mounted to four Grating Array Structures (GAS), which in turn mount to four outer modules in the Flight Mirror Assembly

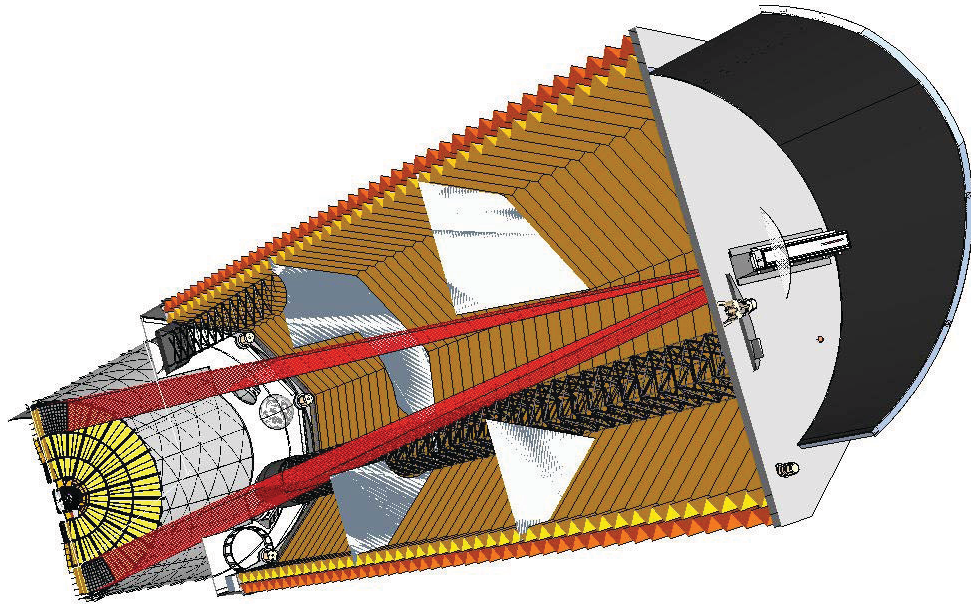


Figure 5. Cutaway of an IXO model, showing the paths of x rays diffracted from the CAT gratings (mounted to the FMA; yellow) onto the CCD camera (mounted to the FIP; grey) in red. Figure courtesy of David Robinson.

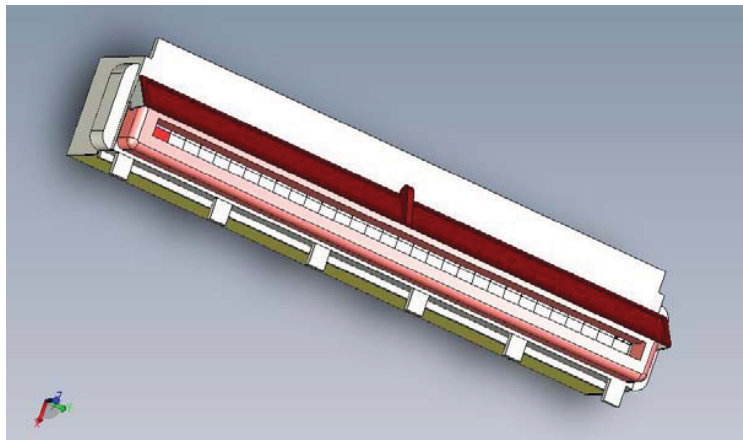


Figure 6. CAD model of the camera assembly, holding a linear array of 32 CCDs.

Table 1. Alignment tolerance estimates for the three most sensitive degrees of freedom. Translation along x and y, as well as rotation around the x-axis (grating yaw), have much more relaxed tolerances.

Translation along z	0.394 mm	
Grating roll (z)	14.3 arcmin	limited by 1/4 of CCD width
Grating pitch (y)	6-20 arcmin	depending on β_m

(FMA), covering approximately $2 \times 30^\circ$ in azimuth. Each grating facet is comprised of an invar frame ($\sim 6 \times 6$ cm²) that supports a 500 micron thin, highly structured silicon membrane, fabricated from silicon-on-insulator (SOI) wafers. Frames are mounted to the GAS via single-point mounts similar to the case of the HETGS on Chandra. GAS and frames are lightweighted and optimized for minimum blockage, while ensuring structural stability. The GAS are machined such that the grating facet centers will conform to a common Rowland torus and be properly aligned.

Mass estimates for the whole grating assembly range from 5-9 kg, depending on the material choice for the GAS. This low mass makes it easy to mount the grating assembly as far as possible from focus, which in turn leads to maximum dispersion and resolution on the camera. The camera mass is dominated by shielding and is estimated to be about 41 kg, including DEA and DPA. Average power consumption of camera and electronics is estimated around 110 W.

Alignment tolerance estimates for individual grating facets listed in Table 1 were derived asking the following question: A resolution of 5000 on blaze corresponds to a PSF width of about 210 micron in the dispersion direction on a CCD. How large of a grating facet misalignments results in a line shift of no more than 10% of 210 micron in the dispersion direction?

Due to the transparency of the CAT gratings at higher energies the grating assembly can be *permanently* mounted in the telescope beam without reducing the effective area at higher energies (6 keV) below mission requirements.

5. FABRICATION OF 200 NM-PERIOD CAT GRATINGS

The CAT grating design requires the fabrication of thousands of accurately spaced, tens of nanometer-thin high-aspect ratio freestanding grating bars with nanometer-smooth sidewalls. Our fabrication process was described in detail previously.²³⁻²⁵ It is based on <110> silicon-on-insulator (SOI) wafers with a device layer thickness equal to the desired grating thickness d .²³ The four main process steps are front side patterning and image reversal, backside patterning and etching, front side etching, and supercritical drying. The front side patterns consist of a chrome mask that defines a coarse support mesh (level I supports), and a silicon nitride mask for the CAT grating bars, generated by scanning-beam interference lithography²⁶ (SBIL). The front side etch in potassium hydroxide (KOH) solution relies on the high etch anisotropy between {111} and {110} planes of silicon, which is highly dependent on the precise alignment between the nitride CAT grating patterns and the silicon crystal planes. The back side etch defines a frame for 3×3 mm² CAT grating prototypes (see Fig. 8(a)). For larger gratings this etch will define a coarser support mesh (level II supports).

We have previously reported on CAT gratings with 200 nm period and nominally 4 micron depth (S4 samples). Recently we have successfully fabricated CAT gratings of the same period with 6 micron depth (S6 samples). Grating bar cross sections are not rectangular, but appear to be slightly trapezoidal (sidewall angle $\sim 0.08^\circ$ from normal), since the top is etched much longer than the bottom. Figs. 8(c) and (d) show scanning electron micrographs (SEM) of various views of two recent samples, one with an average bar width $\langle b \rangle \sim 38$ nm (S6A), the other with $\langle b \rangle \sim 48$ nm (S6B), resulting in average aspect ratios $d / \langle b \rangle$ of 158 and 125, respectively.

The level I supports are currently etched at the same time as the CAT grating bars in KOH. This has the disadvantage that the etch also stops at other, non-vertical {111} planes, which leads to significant broadening of the support bars with increasing etch depth, and concurrent narrowing of the slots between the grating bars (see Fig. 8(b)). We have developed and are presently improving upon other anisotropic etch processes that are

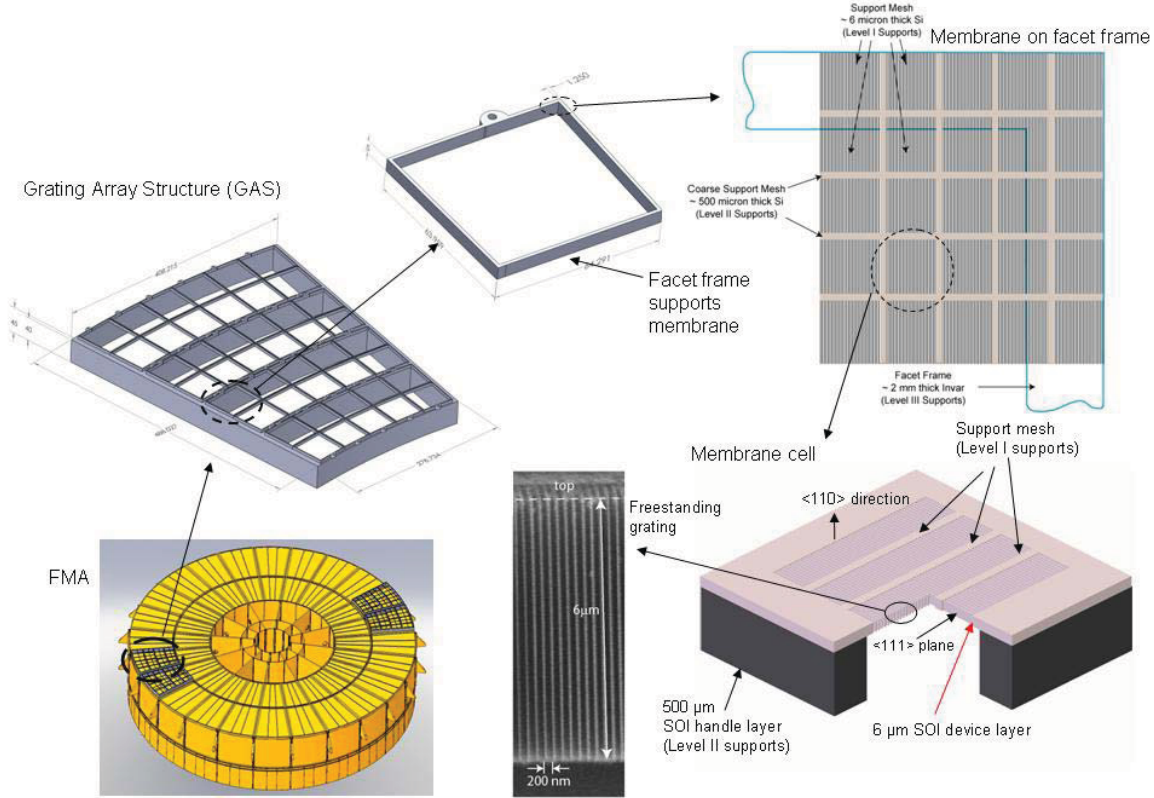


Figure 7. Structural hierarchy of grating assembly.

insensitive to silicon crystal orientations. Those processes, which usually lead to rougher sidewalls, can be used to vertically pre-etch support mesh and CAT grating patterns, and will then be followed by a short KOH etch to “polish” the sidewalls to the necessary smoothness.²⁵

6. SOFT X-RAY DIFFRACTION FROM 200 NM-PERIOD CAT GRATINGS

We present preliminary results on x-ray tests of an S4 sample and sample S6B. Both samples were tested at beam line 6.3.2 of the Advanced Light Source at Lawrence Berkeley National Laboratory in the same setup as described in Ref. 8.

The thickness of the device layer on sample S4 was quoted as 4 micron but turned out to be only about 3.3 - 3.5 micron. After KOH etching the grating bar width varied from ~ 42 nm at the top to ~ 44 nm at the bottom, resulting in a sidewall angle estimate of about 0.02° , and an average duty cycle ($\langle b \rangle / p$) of 0.215. The open gap between the widest parts of the level I supports was a record 48% of the support mesh period. Sample S4 was held at $\alpha \sim 2.6^\circ$ relative to the x-ray beam, which is close to the angle for optimum “filling” of the gaps between grating bars ($d = a / \tan \alpha$). At such a relatively large angle of incidence the critical wavelength for which $\alpha = \theta_c(\lambda)$ is $\lambda \sim 1.82$ nm (0.68 keV). This means that towards this and shorter wavelengths x rays will be weakly reflected from the sidewalls and transmit in 0^{th} order instead (see Fig. 9, and Fig. 6 in Ref. 9). Fig. 9 shows a preliminary comparison of measured diffraction efficiency and theoretical predictions based on a rigorous coupled wave analysis (RCWA)²⁷ model without support mesh. No error bars are given at this time, since the normalization factors and their uncertainties have not yet been fully modeled. Analysis of uncertainties in the

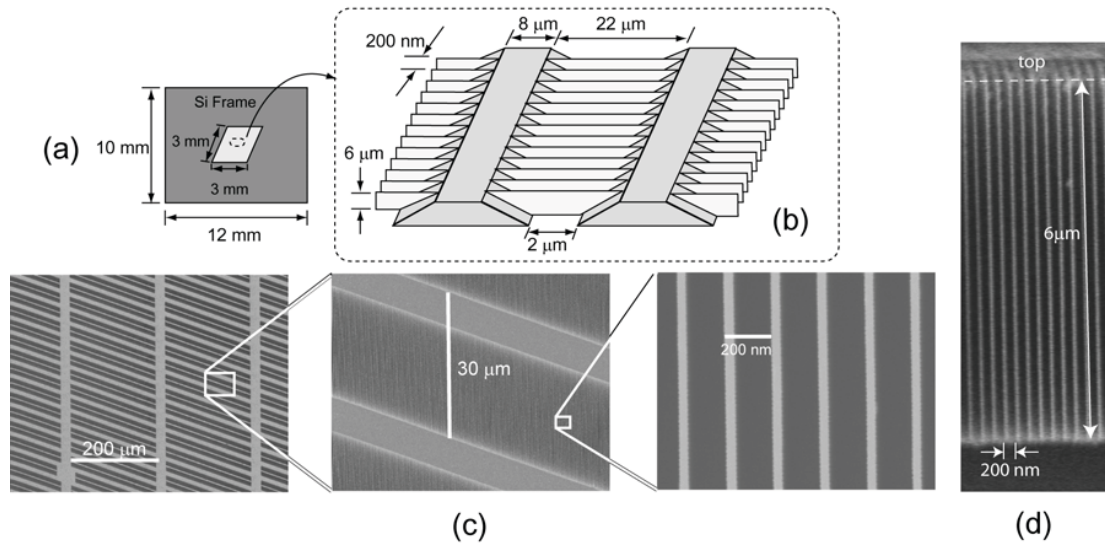


Figure 8. Fabrication results. (a) Schematic top view of a CAT grating sample. (b) Schematic (not to scale) of CAT grating bars (white) and level I support mesh (grey). (c) Top view SEM images from sample S6B at various magnifications, showing level I support grid and CAT grating bars. (d) SEM image of cleaved cross section from sample S6A, showing the high aspect ratio of the CAT grating bars.

geometrical parameters and the modeling of partial transmission through the variable-thickness support mesh are in progress. Nevertheless there is encouraging agreement between theory and experiment.

Fig. 10(a) shows raw detector scan data from sample S6B at different values of α ranging from $+2.74^\circ$ to -2.74° , nicely displaying the blazing effect and the insensitivity of diffraction angles to grating rotation. Again, blazing is strong and 0^{th} order transmission is weak near the condition $d = a/\tan \alpha$, while blazing gets weaker and 0^{th} order transmission increases towards larger angles.

IXO requirements ask for high diffraction efficiency for energies up to 1 keV ($\lambda \geq 1.24$ nm), which is why our goal is the fabrication of optimized CAT gratings with $\alpha \leq 1.5^\circ$. Fig. 10(b) shows raw x-ray data from sample S6B with $\alpha = 1.14^\circ$, and for the first time demonstrates effective blazing at wavelengths down to 0.97 nm (~ 1.28 keV, which is the highest energy available at beam line 6.3.2). The high intensity of orders $0, \pm 1$ at shorter wavelengths is due to the increasing transparency of grating bars and support mesh. For sample S6B the latter makes up about 95% of the area and therefore contributes significantly to 0^{th} order transmission at higher energies.

7. DISCUSSION, SUMMARY, AND OUTLOOK

We have presented a Critical-Angle Transmission Grating Spectrometer concept that meets or exceeds the IXO science requirements for high-resolution soft x-ray spectroscopy. The spectrometer is centered around CAT gratings, which merge the advantages of the transmission geometry with those of blazed reflection gratings. Fabrication of CAT gratings has progressed to achieve the geometrical grating bar parameters suitable for IXO. X-ray tests have shown predicted blazing in excess of the wavelength band required for IXO.

Current and future fabrication efforts are directed at increasing CAT grating area relative to support mesh area, increasing the overall grating area, and improving process yield.

The CATGS design is based on Chandra HETGS heritage and adapted for blazed transmission gratings. Ray trace studies predict spectral resolution in excess of 3000 and are being continued to further optimize the design. Configuration studies have resulted in a realistic instrument design with promising performance and modest use

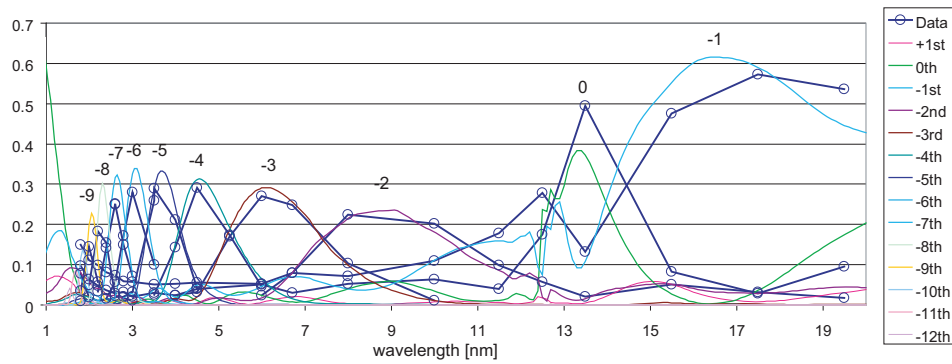


Figure 9. Measured diffraction efficiency of sample S4 for diffraction orders 0 through -9 (data points), and theoretical predictions based on RCWA (lines). See text for details.

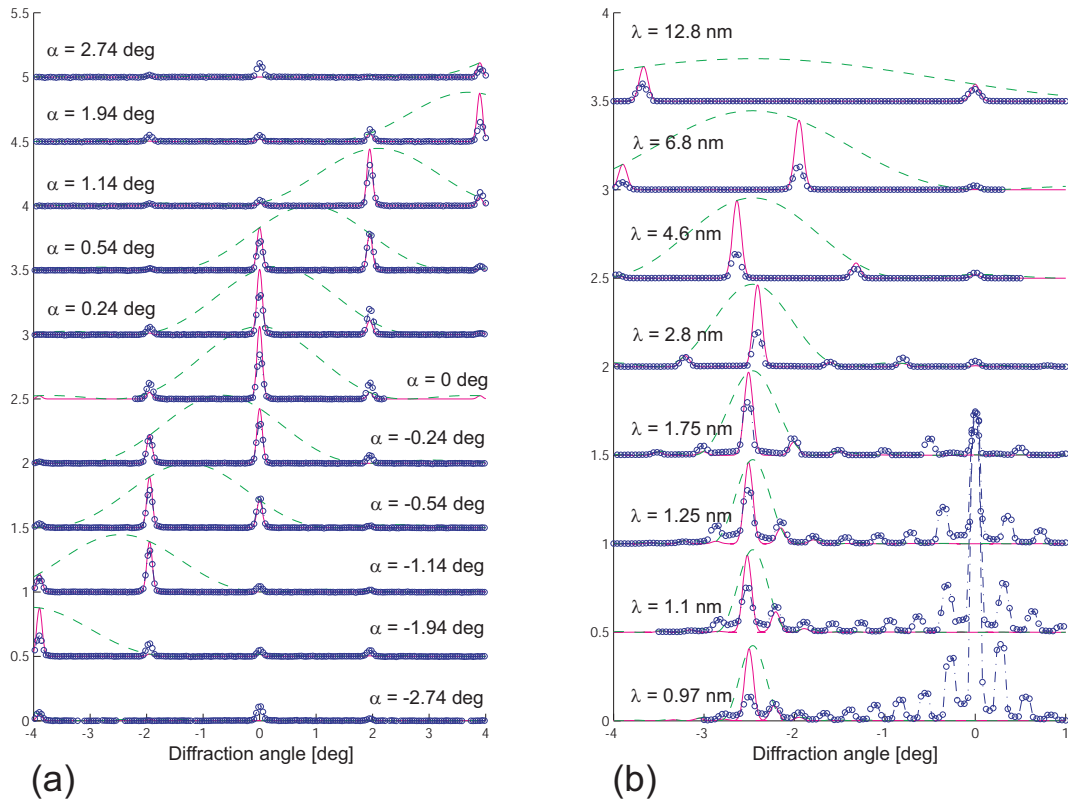


Figure 10. X-ray diffraction data from sample S6B. Circles are data points, solid lines show predictions of the simple model discussed in the text, and dashed lines mark the blaze envelope. Normalization is arbitrary. (a) Detector scans taken at different angles α between the incident synchrotron beam ($\lambda = 6.8$ nm) and the grating normal. The blaze peak moves as 2α . (b) Detector scans at $\alpha = 1.14^\circ$ for different wavelengths.

of resources (mass, power). Grating coverage was matched to the FMA module sizes of the segmented slumped glass optic approach by Zhang.²⁸ However, the effective grating area could easily be increased by extending grating coverage towards inner mirror shells with minimal increase in mass. Area could also be increased in the azimuthal direction, since there is some margin before sub-aperturing fails to boost resolution by a factor of $\sim 1.5 - 2$. Furthermore, a “copy” of the CATGS could be implemented 90° rotated in azimuth (including camera), which would double the effective area. All together the effective area could realistically be increased to above $8,000 \text{ cm}^2$ with the current FMA design.

ACKNOWLEDGMENTS

We gratefully acknowledge technical support from R. C. Fleming (Space Nanotechnology Laboratory), as well as facilities support from the Nanostructures Laboratory and the Microsystems Technology Laboratories (all at MIT). We also thank Eric Gullikson for his support for the x-ray measurements at the Advanced Light Source, and Andrew Rasmussen and Kathryn Flanagan for helpful discussions on the tilted Rowland torus, as well as the Integrated Design Lab at Goddard Space Flight Center. Various parts of this work were supported by NASA grants NNX07AG98G, NNX08AI62G, and NNX09AE82A, and by the Kavli Foundation through a grant from the Kavli Instrumentation and Technology Development Fund.

REFERENCES

- [1] F. B. S. Paerels and S. M. Kahn, “High-resolution x-ray spectroscopy with Chandra and XMM-Newton,” *Ann. Rev. Astron. Astrophys.* **41**, 291-342 (2003).
- [2] See for example <http://ixo.gsfc.nasa.gov/>.
- [3] J. N. Bregman, “The search for the missing baryons at low redshift,” *Ann. Rev. Astron. Astrophys.* **45**, 221-259 (2007).
- [4] See for example R. J. Williams *et al.*, “Probing the local group medium toward Markarian 421 with Chandra and the far ultraviolet spectroscopic explorer,” *Astrophys. J.* **631**, 856-867 (2005).
- [5] See for example Y. Yao, M. A. Nowak, Q. D. Wang, N. S. Schulz, and C. R. Canizares, “Limits on Hot Galactic Halo Gas from X-Ray Absorption Lines,” *Astrophys. J. Lett.* **672**, L21-L24 (2008).
- [6] See for example D. P. Huenenmoerder, J. H. Kastner, P. Testa, N. S. Schulz, and D. A. Weintraub, “Evidence for accretion in the high-resolution X-ray spectrum of the T Tauri star system Hen 3-600,” *Astrophys. J.* **671**, 592-604 (2007).
- [7] K. Flanagan *et al.*, “Spectrometer concept and design for x-ray astronomy using a blazed transmission grating,” *Proc. SPIE* **6688**, 66880Y (2007).
- [8] R. K. Heilmann, M. Ahn, E. M. Gullikson, and M. L. Schattenburg, “Blazed high-efficiency x-ray diffraction via transmission through arrays of nanometer-scale mirrors,” *Opt. Express* **16**, 8658-8669 (2008).
- [9] R. K. Heilmann, M. Ahn, and M. L. Schattenburg, “Fabrication and Performance of Blazed Transmission Gratings for X-Ray Astronomy,” *Proc. SPIE* **7011**, 701106 (2008).
- [10] C. R. Canizares *et al.*, “The Chandra high-energy transmission grating: Design, fabrication, ground calibration, and 5 years in flight,” *PASP* **117**, 1144-1171 (2005).
- [11] A. Rasmussen *et al.*, “Grating arrays for high-throughput soft x-ray spectrometers,” *Proc. SPIE* **5168**, 248-259 (2004).
- [12] R. K. Heilmann *et al.*, “Advances in reflection grating technology for Constellation-X,” *Proc. SPIE* **5168**, 271-282 (2004).
- [13] R. L. McEntaffer *et al.*, “X-ray performance of gratings in the extreme off-plane mount,” *Proc. SPIE* **5168**, 492-498 (2004).
- [14] C.-H. Chang *et al.*, “High fidelity blazed grating replication using nanoimprint lithography,” *J. Vac. Sci. Technol. B* **22**, 3260 (2004).
- [15] J. F. Seely *et al.*, “Efficiency of a grazing-incidence off-plane grating in the soft-x-ray region,” *Appl. Opt.* **45**, 1680-1687 (2006).
- [16] M. Born and E. Wolf, *Principles of Optics* (Cambridge University Press, 1998).
- [17] The term a/p in Eq. (4) of Ref. 8 and Eq. (2) of Ref. 9 should have been replaced with $(a/p)^2$.

- [18] G. Y. Prigozhin, M. W. Bautz, K. C. Gendreau, and G. R. Ricker Jr., "Calibration of x-ray CCDs with an erect-field grating spectrometer in the 0.2- to 1.5-keV band," *Proc. SPIE* **2808**, 260-270 (1996).
- [19] W. C. Cash Jr., "X-ray optics 2: A technique for high-resolution spectroscopy," *Appl. Opt.* **30**, 1749-1759 (1991).
- [20] C.-H. Chang, Y. Zhao, R. K. Heilmann, and M. L. Schattenburg, "Spatial frequency multiplication with multilevel interference lithography," *J. Vac. Sci. Technol. B* **26**, 2135-2138 (2008).
- [21] C.-H. Chang, Y. Zhao, R. K. Heilmann, and M. L. Schattenburg, "Fabrication of 50 nm-period gratings with multilevel interference lithography," *Optics Letters* **33**, 1572-1574 (2008).
- [22] See for example M. W. Bautz *et al.*, "Progress in x-ray CCD sensor performance for the Astro-E2 X-ray imaging spectrometer," *Proc. SPIE* **5501**, 111 (2004); M. W. Bautz, S. E. Kissel, B. J. LaMarr, and G. Y. Prigozhin, "Improved x-ray CCD response at very low x-ray energies," *Proc. SPIE* **6266**, 62662P (2006).
- [23] M. Ahn, R. K. Heilmann, and M. L. Schattenburg, "Fabrication of ultrahigh aspect ratio freestanding gratings on silicon-on-insulator wafers," *J. Vac. Sci. Technol. B* **25**, 2593-2597 (2007).
- [24] M. Ahn, R. K. Heilmann, and M. L. Schattenburg, "Fabrication of 200 nm-period blazed transmission gratings on silicon-on-insulator wafers," *J. Vac. Sci. Technol. B* **26**, 2179-2182 (2008).
- [25] M. Ahn, "Fabrication of Critical-Angle Transmission gratings for high efficiency x-ray spectroscopy," Ph.D. thesis, Department of Mechanical Engineering, Massachusetts Institute of Technology (2009).
- [26] R. K. Heilmann, C. G. Chen, P. T. Konkola, M. L. Schattenburg, "Dimensional metrology for nanometer-scale science and engineering: Towards sub-nanometer accurate encoders," *Nanotechnology* **15**, S504-S511 (2004).
- [27] M. G. Moharam, D. A. Pommet, E. B. Gram, T. K. Gaylord, "Stable implementation of the rigorous coupled-wave analysis for surface-relief gratings - enhanced transmittance matrix approach," *J. Opt. Soc. Am. A* **12**, 1077-1086 (1995).
- [28] W. W. Zhang, "Mirror technology development for the International X-ray Observatory Mission," these proceedings, paper 7437-23.